The Emerald Research Register for this journal is available at
www.emeraldinsight.com/researchregister

The current issue and full text archive of this journal is available at
www.emeraldinsight.com/0961-5539.htm

Received March 2002
Revised May 2003
Accepted June 2003

Investigation of forced convective heat transfer enhancement in the presence of an electric field – a finite element analysis

Asish Bandyopadhyay, Swarnendu Sen and Amitava Sarkar
Department of Mechanical Engineering, Jadavpur University, Calcutta, India
Souvik Bhattacharyya
Department of Mechanical Engineering, Indian Institute of Technology, Kharagpur, India

Keywords *Convection, Finite element analysis, Heat transfer*

Abstract *The effect of electro-convection in a cylindrical flow annulus on heat transfer enhancement has been investigated numerically. Weakly ionized air is considered to be the working fluid throughout this work. The effect of exit boundary condition, considered to be the main hindrance for the numerical solution, has been discussed in detail. The present work shows interesting flow field characteristics, which are in excellent agreement with some other established experiments. The heat transfer enhancement, as reported in this work, appears to be small in view of the low magnitude of the applied voltage but it clearly and surely delineates the trend, i.e. with increase in the strength of the electric field, heat transfer enhances.*

Nomenclature

$\vec{E}$ = electric field vector (electric body force per unit charge)
f_e = electric body force per unit volume
F_e = non-dimensional electric body force $\left(f_e R_2/\rho u_0^2\right)$
H = width of inlet opening $(R_2 - R_1)$
p = pressure
p_r = reference pressure
Pr = fluid Prandtl number $(\mu c_p/K)$
Re = flow Reynolds number $(\rho u_0 R_2/\mu)$
T_i = temperature of fluid at inlet
T_ω = wall temperature
u_0 = reference velocity
u,v = velocity components along z, r directions, respectively
U,V = non-dimensional velocity components along Z, R directions, respectively
V = also used to indicate applied voltage

Greek symbols

ρ = density
ρ_e = charge per unit volume
ψ = non-dimensional stream function
ε = permittivity of the working fluid
ε_0 = absolute permittivity

Subscript

ω = wall

International Journal of Numerical Methods for Heat & Fluid Flow
Vol. 14 No. 3, 2004
pp. 264-284
© Emerald Group Publishing Limited
0961-5539
DOI 10.1108/09615530410517959

Introduction

During the last decade, significant amount of research work on electrohydrodynamically (EHD) enhanced heat transfer and mass transport has been reported by researchers around the world. Rapid control of performance by varying the applied electric field, simple design, low power requirements and absence of sound or vibration are said to be attractive advantages of the application of EHD. Its application in the fields of single- and multi-phase flows is being reckoned as an emerging area in the field of heat and mass transfer. The enhancement of single-phase heat transfer processes, especially in gaseous systems, is an area where researchers and designers spend a great deal of effort. The need to improve the heat transfer rates was made imperative by the ever-increasing requirement for smaller and more cost-effective thermal systems. In single-phase heat transfer, the boundary layers that form on the thermally active surfaces offer a significant resistance to the flow of heat. Enhancing techniques are therefore employed to alter the boundary layer structure of the flow and in laminar or free convective situations, to increase the flow velocity. EHD aims at producing strong corona winds that result in lowering the thickness of thermal boundary layer thus augmenting heat transfer. The corona wind was first discovered by Hauksbee (1719) and was subsequently more rigorously studied by Chattock (1899). Analysis by Robinson (1961) and Steutzer (1959) resulted in a basic understanding of the fluid mechanics of the phenomenon. While Steutzer (1959) presented a theoretical analysis of ion-drag phenomena, Robinson (1961) extended the results of Steutzer (1959) by applying Bernoulli's equation and showed that the corona wind velocity was proportional to the square root of current. Marco and Velkoff (1963) were the first to examine the application of the corona wind to heat transfer enhancement. They produced a wire generated corona wind, which impinged on the bottom of horizontal plate; this resulted in heat transfer coefficient that were six times the free convection value. O'Brien and Shine (1967) followed with an investigation into the effects of pressure and gas type. They found that heat transfer enhancement could not occur below an electrode-specific threshold atmospheric pressure. A maximum local heat transfer enhancement, at atmospheric pressure of 8.5 times the no-field value was reported. These classical observations (Chattock, 1899; Hauksbee, 1719; Marco and Velkoff, 1963) led to a series of subsequent intensive research in the field of heat transfer enhancement by employing EHD technique.

Experimental studies were also conducted on both internal and external flows. Soon it was established that EHD effects are most significant in situations where flow is in the laminar regime. For high turbulent flows, the electrically induced effects become swamped in the presence of turbulence induced eddy-diffusivity effects. An extensive review of literature on EHD enhancement of convective heat transfer can be found in the work of Zia (1989). It has been indicated therein that the prospects of EHD enhancement in forced

convection of gases is yet to be fully explored. However, Mizushina *et al.* (1976) conducted experiments on EHD augmented forced convection in an annulus with air as the working fluid. They examined the effects of both positive and negative field polarities. They were also successful in correlating augmented Nusselt numbers and friction factors in terms of the ratio of ion-drag forces to viscous forces in the bulk flow. Fujino *et al.* (1989) studied augmentation of laminar forced convection heat transfer in a channel flow by employing a transverse dc electric field with R113 as the working fluid. Ohadi *et al.* (1991) experimentally studied the effect of corona discharge on forced convection heat transfer in a tube with air as the working fluid. Single- and double-electrode configurations were used in their work. They concluded that significant heat transfer enhancement are possible, in the case of a single electrode, for only in the laminar and transitional flow regimes while, on the other hand, with a two electrode configuration, enhancement in heat transfer could be extended to the turbulent flow regimes as well. Two recent review papers (Allen and Karayiannis, 1995; Seyed-Yagoobi and Bryan, 1999) describe the state-of-the-art survey of EHD-based heat transfer enhancement encompassing typical application areas like multi-phase flows, natural convection, etc.

From what has been described earlier, it appears that although considerable effort has been emfployed for experimental determination of heat transfer enhancement, little has been done towards it from the viewpoint of numerical simulation. In this work, an attempt will be made to demonstrate the heat transfer enhancement purely from the viewpoint of numerical analysis. For this purpose, the case of flow of air through an annulus, as described by Ohadi *et al.* (1991), has been chosen with the inner cylinder being assumed to represent the high-voltage wire. Since it has been stated earlier that the effect of EHD-based heat transfer enhancement is most pronounced in the laminar regime, the present work and subsequent discussion will be limited to lower values of the Reynolds number.

Interaction of the electric field with forced convection

Generally, the flow produced by applying a dc electric field to a weakly-ionized fluid may be pictured as a free jet discharged into a fluid of the same type. The net effect can be used to destabilize the thermal boundary layer on the heat transfer wall and, therefore enhance the heat transfer coefficient. As a consequence of this field, the electric body force density acting on the molecules of a fluid consists of three terms (Melcher, 1981) as shown below:

$$\vec{f}_{\mathrm{e}} = \rho_{\mathrm{e}}\vec{E} - \frac{1}{2}E^2\vec{\nabla}\varepsilon + \frac{1}{2}\vec{\nabla}\left[E^2\rho\left(\frac{\partial\varepsilon}{\partial\rho}\right)_{\mathrm{T}}\right] \tag{1}$$

The three terms in equation (1) represent three different kinds of force densities acting on the fluid. The first term represents the force acting on the free charges in the presence of an electric field and is known as the Coulomb force. In cases

where the permittivity of the fluid is assumed constant (as in the present case), the second and third terms on the right-hand side of equation (1) become negligible. Under these circumstances, the electric body force is simply the Coulombic force

$$\vec{f}_e = \rho_e \vec{E} \tag{2}$$

Yabe *et al.* (1978) has shown that the Coulombic force was the principal force in producing corona wind for positive discharge in a wire-and-plate configuration, with nitrogen as the working fluid.

Now that the electrical force field has been explicitly expressed, it remains to determine the expressions for ρ_e and $\vec{E}$ in terms of system dimensions and applied electrical field. Details of the derivation have been described in the Appendix. It is seen therefrom that the electrical body force per unit volume of the fluid along the radial direction is given by

$$f_e(r) = -\frac{\varepsilon_0}{r^3}\left[\frac{\phi(R_2) - \phi(R_1)}{\ln R_1/R_2}\right]^2 \tag{3}$$

Equation (3) is a general description of the variation of $f_e(r)$ when the electrode length is infinite. For electrodes of finite length, the electric force field is expected to be a function of r and Z. However, a "long electrode length" had to be avoided in this study to avoid complications associated with exit boundary conditions – a matter adequately discussed later.

Because of the axisymmetric nature of the electric field force, f_e, is expected to influence the r-momentum equation only and will appear as a source term in that equation, as discussed below.

Governing equations, boundary conditions and the numerical scheme

For steady, incompressible, two-dimensional laminar flow, the conservation equations (in the axisymmetric case) are as follows.

Continuity:

$$\frac{1}{r}\frac{\partial(rv)}{\partial r} + \frac{\partial u}{\partial z} = 0 \tag{4a}$$

z-momentum:

$$\rho\left[u\frac{\partial u}{\partial z} + v\frac{\partial u}{\partial r}\right] = -\frac{\partial p}{\partial z} + \mu\left[\frac{\partial^2 u}{\partial z^2} + \frac{\partial^2 u}{\partial r^2} + \frac{1}{r}\frac{\partial u}{\partial r}\right] \tag{4b}$$

r-momentum:

$$\rho\left[u\frac{\partial v}{\partial z} + v\frac{\partial v}{\partial r}\right] = -\frac{\partial p}{\partial r} + \mu\left[\frac{\partial^2 v}{\partial z^2} + \frac{\partial^2 v}{\partial z^2} - \frac{v}{r^2} + \frac{1}{r}\frac{\partial v}{\partial r}\right] + f_e(r) \tag{4c}$$

Energy:

$$\rho c_p \left[u \frac{\partial T}{\partial z} + v \frac{\partial T}{\partial r} \right] = k \left[\frac{\partial^2 T}{\partial z^2} + \frac{\partial^2 T}{\partial r^2} + \frac{1}{r} \frac{\partial T}{\partial r} \right] \tag{4d}$$

These equations are made dimensionless with the introduction of the following non-dimensional quantities:

$$U = \frac{u}{u_0}; \quad V = \frac{v}{u_0}; \quad Z, R = \frac{z, r}{R}; \quad P = \frac{p - p_r}{\rho u_0^2}; \quad \theta = \frac{T - T_i}{T_\omega - T_i}$$

The conservation equations in dimensionless form are as shown below:

$$\frac{V}{R} + \frac{\partial V}{\partial R} + \frac{\partial U}{\partial Z} = 0 \tag{5a}$$

$$U \frac{\partial U}{\partial Z} + V \frac{\partial U}{\partial R} = - \frac{\partial P}{\partial Z} + \frac{1}{\mathrm{Re}} \left(\frac{\partial^2 U}{\partial Z^2} + \frac{\partial^2 U}{\partial R^2} + \frac{1}{R} \frac{\partial U}{\partial R} \right) \tag{5b}$$

$$U \frac{\partial V}{\partial Z} + V \frac{\partial V}{\partial R} = - \frac{\partial P}{\partial R} + \frac{1}{\mathrm{Re}} \left(\frac{\partial^2 V}{\partial Z^2} + \frac{\partial^2 V}{\partial R^2} - \frac{V}{R^2} + \frac{1}{R} \frac{\partial V}{\partial R} \right) + F_e \tag{5c}$$

$$U \frac{\partial \theta}{\partial Z} + V \frac{\partial \theta}{\partial R} = \frac{1}{\mathrm{Re} \cdot \mathrm{Pr}} \left(\frac{\partial^2 \theta}{\partial Z^2} + \frac{\partial^2 \theta}{\partial R^2} + \frac{1}{R} \frac{\partial \theta}{\partial R} \right) \tag{5d}$$

The flow domain is shown in Figure 1.

Since the flow is assumed to be axisymmetric, we concentrated on the upper half of the flow domain and considered it as the computational domain, which is shown in Figure 2. The hydrodynamic and thermal boundary conditions are marked therein.

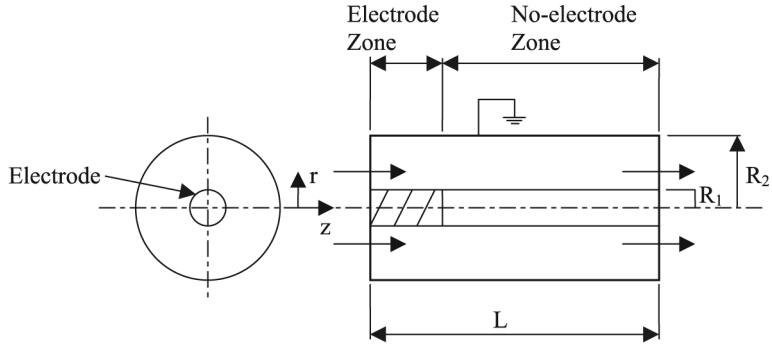

Figure 1.
Flow domain

A large length of the computational domain had to be considered so that the flow becomes fully developed at the domain exit. The pressure reference point is chosen at a node on the exit plane of the computational domain. The effect of these boundary conditions will be discussed in detail in the subsequent section.

The non-dimensional governing equations (5(a)-(d)) are discretized by standard Galerkin method. Since the energy equation (5(d)) is not linked with the momentum equations, the later equations are treated by Newton-Raphson method and the discretized equations are solved by a frontal solver. The advantage of the Newton-Raphson method lies in the fact that for attaining a prescribed convergence level, not more than six iterations are required for a given set of input parameters. By "prescribed convergence level", in the context of the present work, it is implied that the difference in the values of a variable, for two successive iterations, does not exceed 10^{-7}. Finite element formulation of the constitutive equations starts with defining variables at the nodes. In the present work, an eight-noded isoparametric quadrilateral element has been used throughout for the purpose of discretization. To avoid the spurious modes of pressure rise, pressure is defined only at the corner nodes while other variables are defined at all nodes. During the discretization process, velocity shape functions are used to weight the momentum and energy equations while the pressure shape function is used to weight the continuity equation. The detail of the procedure has been described by Nag *et al.* (1993). Once the velocity field is obtained from the solution of equations (5(a)-(c)), the temperature field is obtained directly from the solution of equation (5(d)). The local Nusselt number at the hot wall at $R = 1$ is defined by the following relation:

$$-K\frac{\partial T}{\partial r}\bigg|_{r=R_2} = h(T_\omega - T_i) \quad \text{or} \quad \text{Nu}(Z)\bigg|_{R=1} = -\frac{\partial \theta}{\partial R}|_{R=1} \tag{5e}$$

Now, a few words about the selection of the reference temperature T_i in the above equation are in order. As far as the heat transfer aspect is concerned, the heat transfer from the hot wall is expected to be governed by $(T_\omega - T_b)$ where T_b is the local fluid bulk temperature. Indeed this is the practice for single-phase forced convection cases. However, as far as the application of this practice to EHD related field is concerned, a few difficulties arise. Ohadi *et al.* (1991) pointed

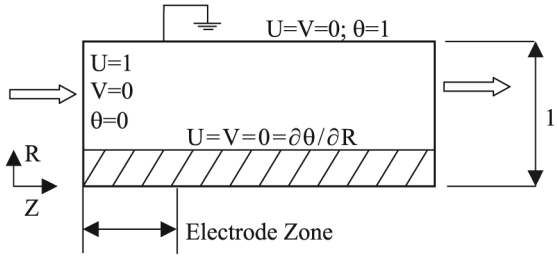

Figure 2.
Computational domain

out that small output (a few millivolts) signal of thermocouples, which would be used for the measurement of bulk temperature, could be easily swamped in the presence of high voltage field. The second major problem, according to them, could be due to the presence of a pointed object such as a thermocouple into the electric field which might result in local distortion of the electric field, and any such distortion of the field would alter the local electrostatic force on the fluid – thus altering the heat transfer rates. Accordingly, they had defined fluid bulk temperature based on the average of temperatures at inlet and outlet sections of the test zone. Fujino *et al.* (1989) calculated $T_b(z)$ by using an energy balance between the inlet section and the z-section for the constant wall heat flux case. It appears that, for the EHD-based heat transfer cases, the concept of reference temperature had been dictated purely by experimental constraints rather than the driving temperature difference concept. However, in the present work, the local bulk temperature of the fluid (defined later) has been used throughout for the purpose of calculation of the heat transfer due to the fact that this temperature can be easily calculated numerically; in addition, comparison with benchmark solutions became easier with its use.

For stream function calculation in (R, Z) co-ordinates, a non-dimensional stream function ψ is introduced such that

$$U = \frac{1}{R}\frac{\partial \psi}{\partial R} \quad \text{and} \quad V = -\frac{1}{R}\frac{\partial \psi}{\partial Z}$$

These satisfy the continuity equation. The nodal values of ψ are calculated from the following Poisson equation.

$$\frac{\partial^2 \psi}{\partial R^2} + \frac{\partial^2 \psi}{\partial Z^2} = U + R\left(\frac{\partial U}{\partial R} - \frac{\partial V}{\partial Z}\right)$$

The inlet boundary conditions are obtained by integrating one of the fundamental relations, described above.

Accordingly,

$$\psi_2 - \psi_1 = \int_{R_1}^{R_2} U(R)|_{Z=0}\, R\, \mathrm{d}R$$

The stream function on the electrode surface has been arbitrarily assigned a value of zero. Exit plane boundary conditions for ψ are easily derivable from the full developed flow conditions.

Results and discussions

Before a detail discussion on the results, a few words about the code validation and grid independence test might be more relevant. Recently, a present code has been developed and we felt that it is necessary to validate the present code

with some standard benchmark result. The standard result, under consideration, corresponds to the asymptotic value of Nusselt number for laminar fully developed flow in a tube under isothermal condition. This value is 3.66 (Kays and Crawford, 1983). The present code yielded the results as described in Table I for two different values of Reynolds number at different mesh sizes.

The non-dimensional length of the computational domain was 100 and the Nusselt number values were based on the tube diameter as the characteristic length and the difference between the wall temperature and the bulk mean temperature was considered as the driving temperature difference for the heat transfer process. It turns out that the 30×18 mesh (i.e. 30 elements in the Z-direction × 18 elements in radial direction) produced the closest approximation to the benchmark value; in addition, Table I also shows that this value, as expected, does not depend on the Reynolds number.

The above code validation study was based on flow through a tube. Since the present problem involves flow through an annulus, a further grid independence study appears to be necessary. For this purpose, the same configuration (Figure 2) has been used. The length of the computational domain is 200 and $R_1/R_2 = 0.00718$. Table II shows the results of such an exercise for a Reynolds number of 500.

In this study, the bulk temperature, θ_b, at any given value of z has been calculated from the following expressions.

$$U_{av} = \frac{2}{\left[1 - \left(\frac{R_1}{R_2}\right)^2\right]} \int_{R_1/R_2}^{1} UR \, dR$$

and

$$\theta_b = \frac{2}{U_{av}\left[1 - \left(\frac{R_1}{R_2}\right)^2\right]} \int_{R_1/R_2}^{1} UR\theta \, dR$$

The local Nusselt number can be calculated from the heat balance at the isothermal surface and is expressed as follows:

Mesh size	Nu_∞ Re = 100	Re = 300
28 × 16	3.680	3.680
28 × 18	3.670	3.700
30 × 16	3.665	3.700
30 × 14	3.675	3.680
30 × 18	3.667	3.667

Table I. Code validation

$$\mathrm{Nu}(Z)\Big|_{R=1} = \frac{2h(Z)R_2}{K} = -\frac{2}{[1-\theta_b(z)]}\frac{\partial\theta}{\partial R}\Big|_{R=1}$$

The average Nusselt Number (Nu_{av}), based on the integration along the length of the isothermal wall of the tube, can be found easily with the help of the local Nusselt number. The above grid independence study clearly delineates the necessity of finer axial discretization and in all subsequent simulation exercises, this procedure was followed. Figures 3 and 4 demonstrate typical distributions of surface pressure, local Nusselt number along the length of the tube. It can be seen that both surface pressure and local Nusselt number distribution experience a sharp drop initially before the surface pressure experiences a linear drop while the local Nusselt number reaches asymptotically a near constant value. The temperature distributions at several axial locations are also shown (Figure 5).

A typical stream line pattern for $\mathrm{Re} = 500$ is shown in Figure 6. It is seen that the streamlines, for a considerable zone along the radial direction, turn inwards initially before becoming almost horizontal in the later part of the annulus. On the contrary, the streamlines near the inner cylinder are deflected slightly outwards (due to the presence of the boundary layer) before becoming parallel to the axial direction.

Now the effect of electrical field will be considered. However, before initiating the discussion on the effect of electric field, a few words about the limitation of full-developed boundary condition at the outlet and necessity of using a large computational domain length may be appropriate. Let us consider the case of the flow through the annulus for $\mathrm{Re} = 1{,}200$ and an electrode length of 25 while the total length of the domain is 250. At the first instance, it may appear that an unusually large length has been considered. This is indeed the case if one does not consider the effect of electric field. However, the situation changes drastically when a moderate electric field is applied to an otherwise fully developed flow without any electric field. Since it is mentioned earlier that the electrode can be considered as a potential generator of the radial velocity component, a comparative study of the radial velocity distribution at the exit planes of the electrode section (i.e. $Z = 25$) and of the domain (i.e. at $Z = 250$) might be instructive. Table III gives details of such a study. It is seen that while there is considerable radial velocity at $Z = 25$ corresponding to no-field

Table II.
Grid independence study of flow through annulus

Grid size	$\mathrm{Nu}_{(\text{at exit plane})}$	Nu_{av}	$\theta_{(\text{exit plane})}$	$U_{\max\ (\text{exit plane})}$
40×12	3.988	9.733	0.7606	1.669
45×10	3.884	9.604	0.7613	1.665
45×8	3.934	9.552	0.7597	1.678
55×8	3.950	9.520	0.7595	1.678
65×8	3.950	9.520	0.7595	1.678

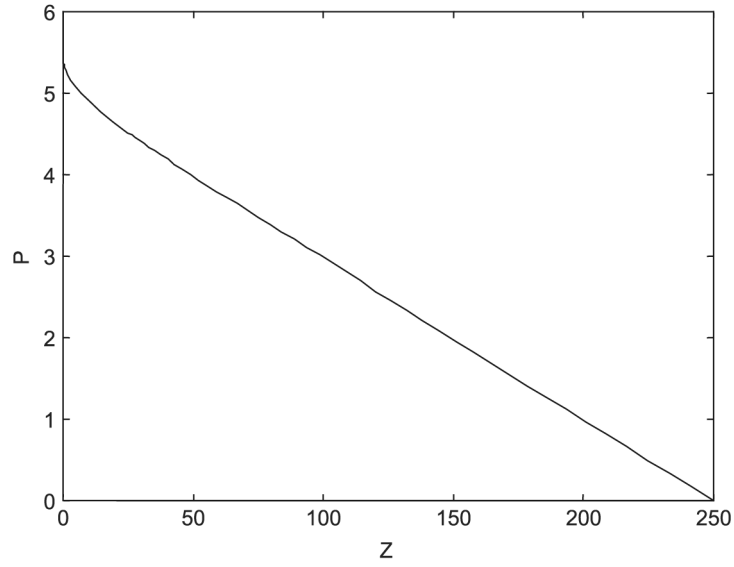

Figure 3.
Surface pressure distribution for Re = 500 and $V = 0$

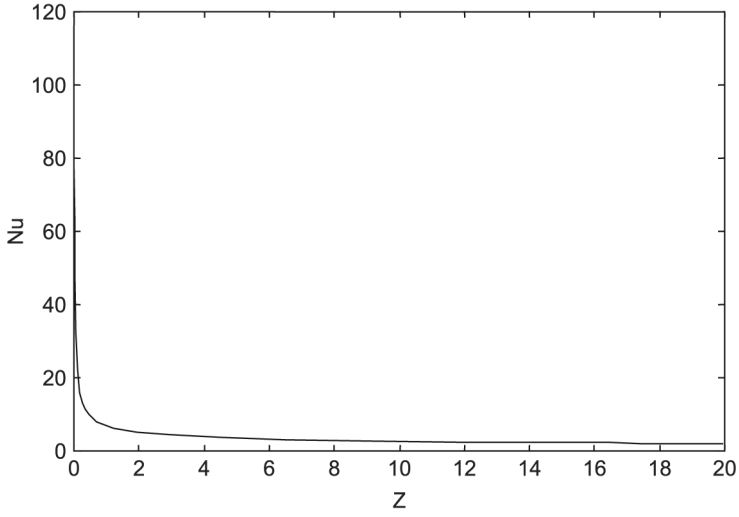

Figure 4.
Distribution of local Nusselt number for Re = 500 and $V = 0$

condition, the situation at $Z = 250$ closely conforms to the fully developed boundary condition. The presence of significant radial velocity components at $Z = 25$ may be ascribed to the fact that this is well within the "developing flow regime". Now, a comparison of V-velocities between the no-field case and the one in which 100 V is applied to the electrode leads to a few interesting observations. It is seen that velocities have changed by at least two orders of magnitude at the indicated locations. This major increase is more predominant

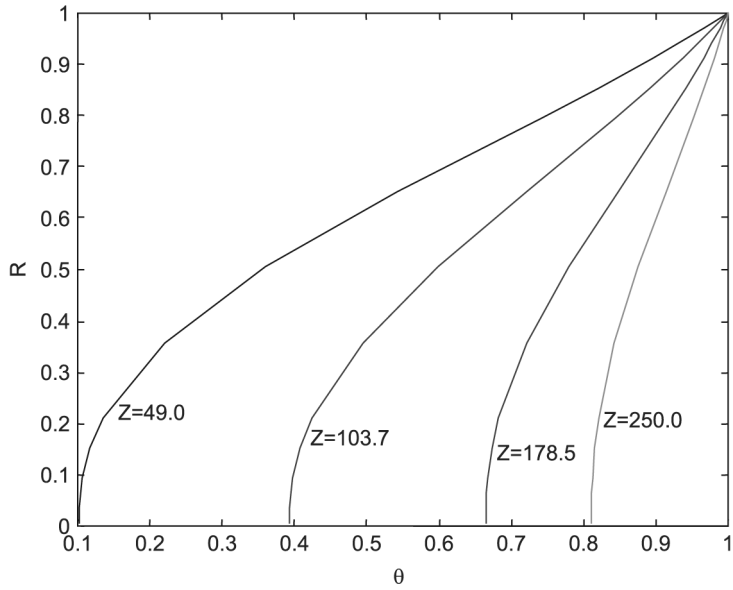

Figure 5.
Temperature distribution at different sections at Re = 500 and $V = 0$

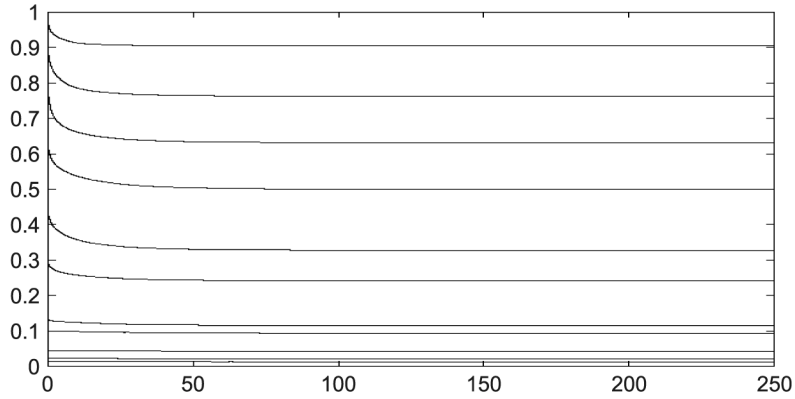

Figure 6.
Streamline pattern for Re = 500 and $V = 0$

in regions close to the electrode. In addition to this, it is further observed that the perturbations produced in the electrode region do not die down even though a large length of the recovery section was provided. In fact, at $Z = 250$, the decrease in radial velocity in the inner cylinder region is compensated by an increase of the same at regions near the outer isothermal cylinder. This directly points to the necessity of having a large length of the computational domain even at low electric field situation. However, the computational cost also increases and a trade-off at this point must be made. It appears that either one will have to accept "small" radial velocity components at the exit plane or will have to be satisfied with an extraordinarily large domain to completely satisfy fully-developed boundary condition. In the present work, the first practice is

	$V = 0$		$V = 100$	
R	$Z = 25$	$Z = 250$	$Z = 25$	$Z = 250$
0.0072	0	0	0	0
0.0218	0.000003	0	0.009693	0.000809
0.0364	0.000001	0	−0.044431	0.001698
0.0656	−0.000024	0	0.015774	0.002856
0.0948	−0.000056	−0.000001	0.005211	0.004157
0.1532	−0.000180	−0.000003	−0.009976	0.004976
0.2116	−0.000328	−0.000001	−0.006772	0.006275
0.3576	−0.000977	−0.000004	0.001329	0.006028
0.5036	−0.001703	0.000017	−0.001605	0.013889
0.6496	−0.001461	0.000054	−0.001754	0.032275
0.7956	−0.000696	0.000040	−0.001216	0.028079
0.8540	−0.000470	0.000016	0.000026	0.010364
0.9124	−0.000186	0.000070	0.000250	0.004311
0.9416	−0.000082	0.000005	0.000109	0.003485
0.9708	−0.000020	0.000002	0.000104	0.001626
0.9854	−0.000004	0.000001	0.000072	0.000632
1.0000	0	0	0	0

Table III. Radial velocity values at axial locations ($Z = 25$ and 250) in the absence/presence of the applied field

followed i.e. results are obtained for different electric fields as long as the maximum value of the radial velocity component remains below 5 per cent of the maximum value of the axial velocity component at the domain exit plane. This compromise points to the fact that all subsequent discussions are only approximate; however, they adequately help in arriving at considerable qualitative agreement with experiments, as will be discussed shortly.

For the purpose of flow visualisation, a flow Reynolds number of 1,200 has been selected; in addition, three streamline patterns are considered – one for no-field condition while the other two are for 100 and 225 V, respectively Figures 7-9. Some interesting features of the flow field, compared with the zero electric field conditions are described below:

(1) Application of electric field produces secondary rolls near the electrode surfaces; the size of these rolls increases in the flow direction. Formation of these secondary rolls near the electrodes pushes other streamlines in the radial direction. This has two-fold consequences – streamlines being more closely packed near the isothermal surface, shear forces on the outer wall increases, resulting in greater pressure drop compared to the no-field case. By the same ground, the thermal boundary layer thickness also decreases resulting in increased heat transfer. This near-electrode flow field structure is in excellent agreement with the experimental work of Fujino *et al.* (1989).

(2) Now, the change in pattern for the streamlines, which are away from electrode surface, may be examined. In sharp contrast to the no-field case, one can notice the presence of ripples in these streamlines when

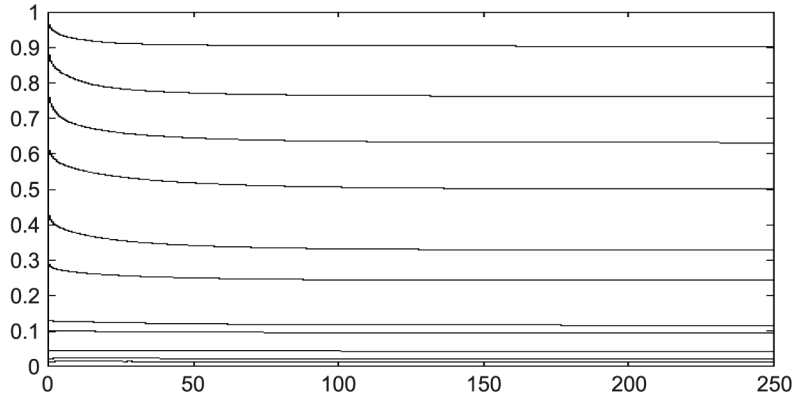

Figure 7.
Streamline pattern for Re = 1,200 and $V = 0$

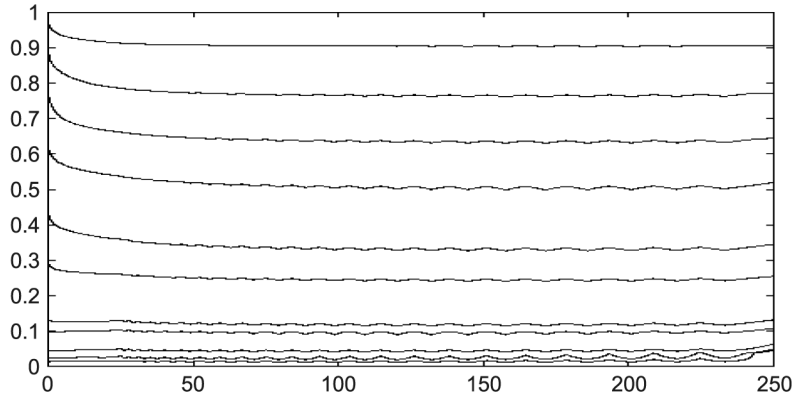

Figure 8.
Streamline pattern for Re = 1,200 and $V = 100$

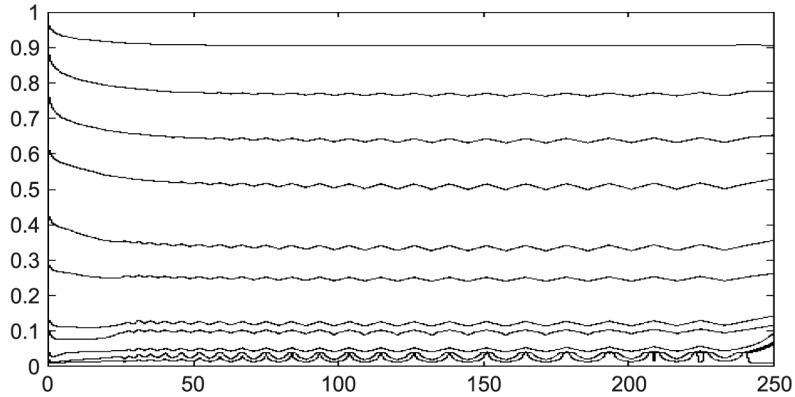

Figure 9.
Streamline pattern for Re = 1,200 and $V = 225$

strong electric field is present. In radial direction, these ripples between the streamlines appear to be in phase while in the axial direction, the wavelength gradually increases with no significant changes in the amplitude. This presumably points to the decay process of these waves in the exit region.

(3) Presence of ripples in flow field streamlines indicates that a greater path length is traversed by the fluid particle in the flow domain compared with no-field case; consequently, it may be imagined that the "residence time" of a fluid particle in the domain increases due to the additional path it has to travel, resulting in "greater time" for increased heat transfer.

(4) Formation of ripples on the streamlines in the electrode zone is mainly dependent on the magnitude of applied voltage and the flow Reynolds number. When Re is high, the perturbations, produced in the electrode zone, by the electric field are swamped away downstream only to re-appear subsequently in the no-field region. For low values of Re, it is expected that the manifestation of ripples should occur over the electrode region. For this purpose, streamline patterns for $\mathrm{Re} = 200$ and an applied field of 125 V has been considered (Figure 10). Ripples, however weak they are, seem to be present; the striking feature is the significant way-ward shift of near-electrode streamlines from the electrode surface. This may be ascribed to the fact that at low Reynolds number, the radial velocity components in the flow-developing region, in association with those generated by the electric field, contribute to the shift of streamlines away from the electrode surface. In brief, the shift may be visualised as the outcome of the race between fluid inertia along the flow direction and that in the cross-stream direction. Once the electrode zone ends (at $Z = 25$), there is a sudden change in the value of the radial velocity components and initiation of formation of secondary rolls takes place.

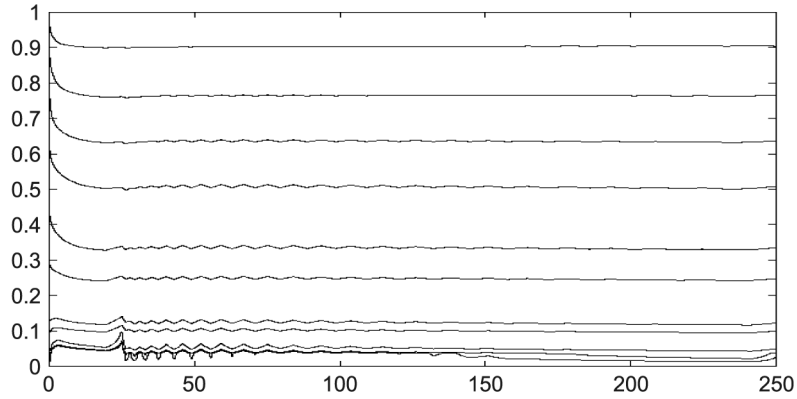

Figure 10.
Streamline pattern for $\mathrm{Re} = 1{,}200$ and $V = 125$

Subsequent to the analysis of flow structure, a few remarks about the pressure distribution on the isothermal surface might be desirable. Figure 11 shows pressure drops in the electrode zone along the isothermal surface for Re = 1, 200. It is seen that, within the range of applied voltage, pressure drop between the inlet and exit section (Δp_E) becomes less compared to the no-field case (Δp_O). This means that lesser pumping work is necessary when electro-convection is present – a fact experimentally established by Fujino *et al.* (1989). This is typical of low voltage regime; the behaviour reverses at higher voltages due to reasons, which are already explained under item (1) earlier. This trend is also reported by Fujino *et al.* (1989).

The variation of local Nusselt number along the isothermal surface for Re = 1, 200 with and without the electric field is shown in Figures 12 and 13. The variation has been split over the length of flow domain to clearly demonstrate the pattern in electrode and no-electrode regions. The electrode region clearly predicts the heat transfer enhancement as the applied voltage is increased. At or near the entry section, the local Nusselt number is expectedly very high; during the later part the local Nusselt number decreases at a lesser rate due to increase of fluid bulk temperature "θ_b". While this is the trend in the electrode region, local Nusselt number exhibited a wavy pattern in the no-electrode region. This is a typical characteristic of the electro-convection phenomena. A close look at the corresponding streamlines (Figures 7-9) would reveal that the streamline near the isothermal surface is almost unperturbed by the electric field effect. The question that logically arises is that, if the flow situation near the isothermal surface has not changed much, what could be the source of the wavy nature of the local heat transfer distribution? This can be

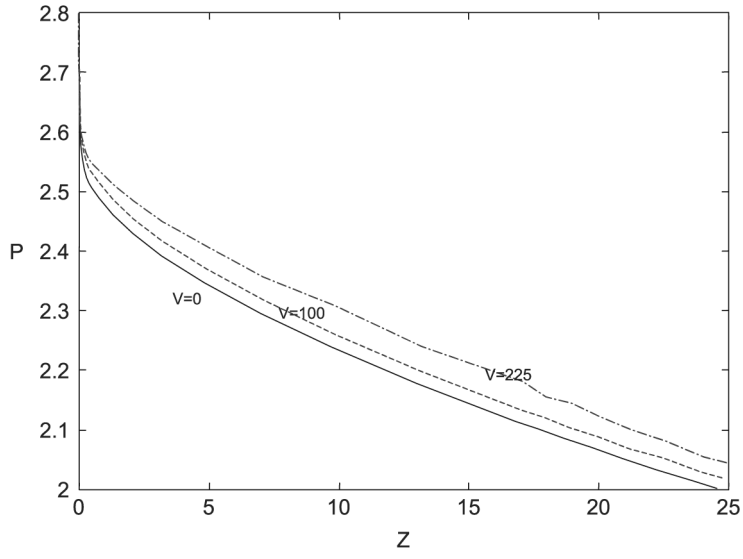

Figure 11.
Variation of surface pressure at Re = 1,200

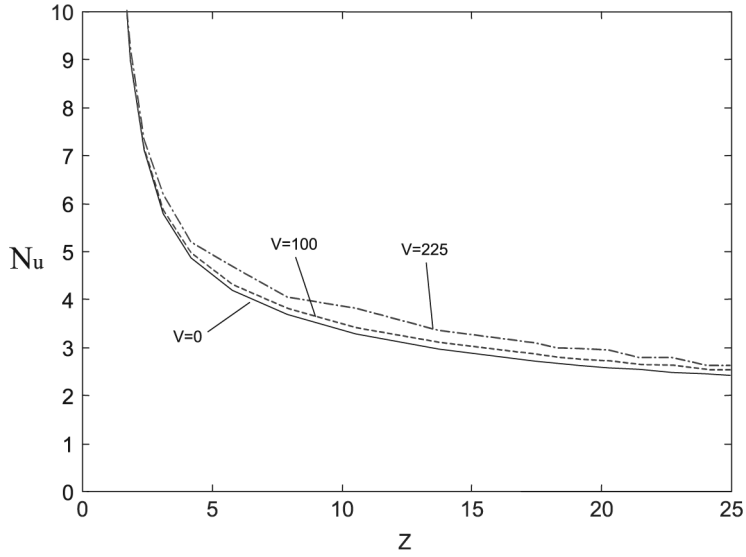

Figure 12.
Variation of local Nusselt number along the isothermal surface at Re = 1,200

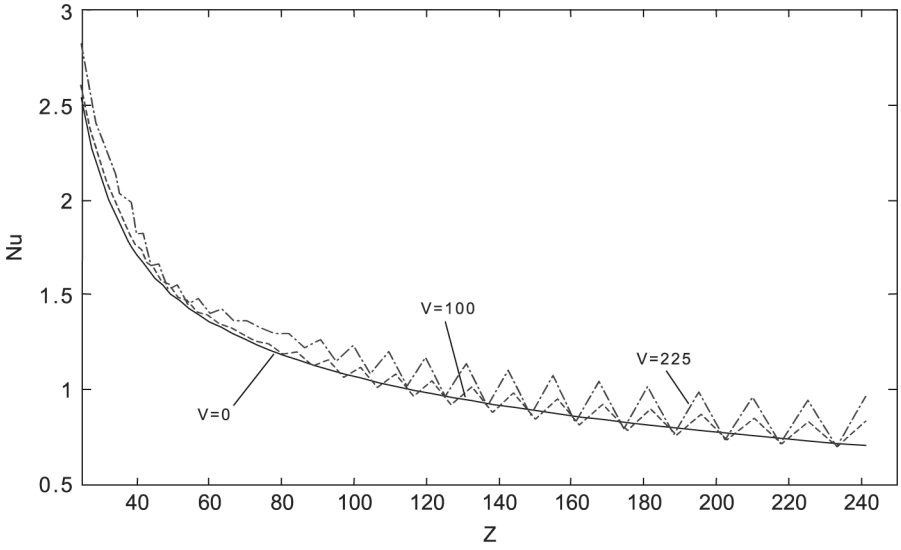

Figure 13.
Variation of local Nusselt number along the isothermal surface at Re = 1,200

best explained by noting that the local Nusselt number depends on the bulk mean temperature of the fluid at a given section, which again takes into consideration the value of bulk velocity at that section. So, although the streamline near the isothermal wall is unaffected by the presence of the field, the ripples in the faraway streamlines considerably influence the heat transfer from the isothermal surface. The effects of these ripples are so strong that at some locations, the local Nu falls below the no-field value while at others it

overshoots the no-field value considerably – the average effect, as can be verified, is enhancement of heat transfer.

Finally, the isothermal patterns for three cases with Re = 1, 200 are shown in Figures 14-16; the three cases correspond to the no-field condition and applied voltage of 100 and 225 V. The most important point to be noticed is the closer packing of isotherms near the isothermal surface with increasing voltage – a phenomena primarily responsible for augmentation of heat transfer from the outer isothermal surface. The crowding of isotherms at the inlet plane do justify large value of heat transfer coefficient observed here; this is due to the existence of a singularity arising out of the specification of the thermal boundary condition in that region. Other noticeable feature is the presence of ripples in isotherms – an expected characteristic in forced convection phenomena where the temperature field is determined from an existing velocity field.

Table IV represents a typical collection of heat transfer data for Re = 1,200 and different applied voltages. It is seen that as voltage increases, the average Nusselt number in the electrode region increases: the same is the case with the

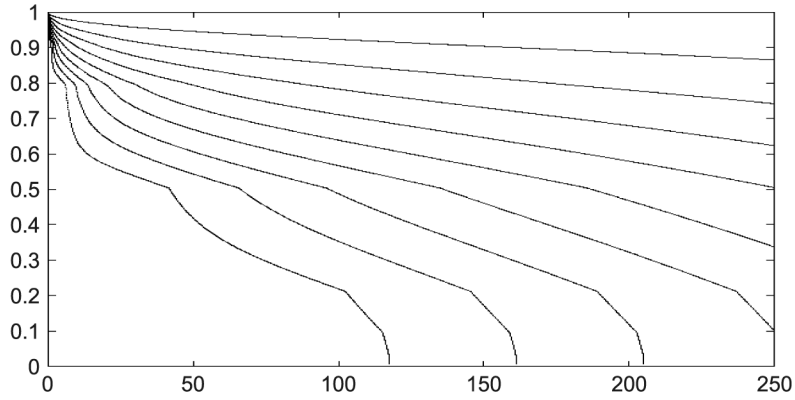

Figure 14.
Isothermal pattern for Re = 1,200 and $V = 0$

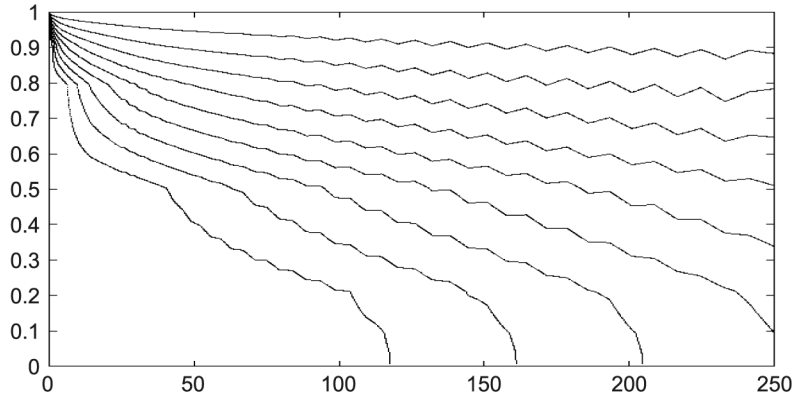

Figure 15.
Isothermal pattern for Re = 1,200 and $V = 100$

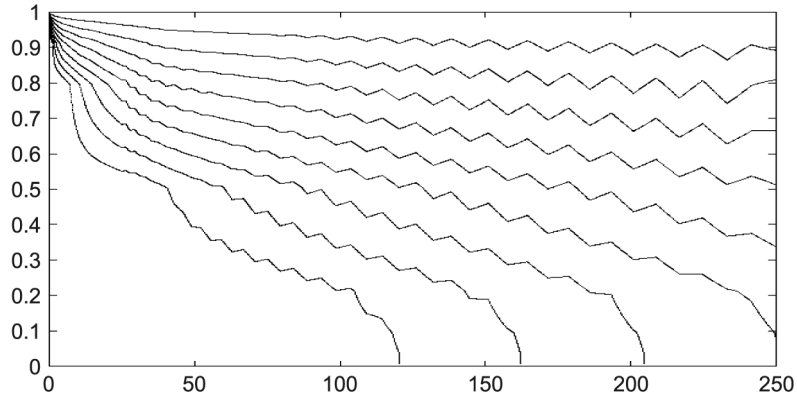

Figure 16.
Isothermal pattern for Re = 1,200 and $V = 225$

Applied voltage (V)	Nu_{av} (electrode region)	Nu_{av} (total isothermal surface)
0	11.440	5.145
100	11.503	5.179
125	11.543	5.192
150	11.563	5.155
225	11.598	5.176

Table IV.
A typical result of heat transfer enhancement

average Nusselt number for the entire surface except the case when the applied voltage is 150. In this case, only the average Nusselt number decreased to 5.155; as the voltage was further increased, the Nu - value also increased. Such trends are also reported in the experimental works of Fujino *et al.* (1989) and Ohadi *et al.* (1991). The same trend has been observed for Re $= 1,000$ at $V = 150$.

Conclusion

This work has numerically demonstrated the effect of electro-convection under forced flow condition. The typical flowfield patterns, which have never been numerically investigated, have been addressed with adequate attention. Excellent qualitative agreement with some established experimental work marked the correctness of the numerical approach. Formation of secondary rolls and presence of ripples in the streamlines are found to be a typical characteristic of the electro-convection process. Unlike the EHD process, where the corona wind is generated and heat transfer enhancement of 200 per cent has been reported, the heat transfer enhancement in the present case is of the order of a few per cent. This small enhancement is attributable to the small value of the applied voltage. The other important aspect is the problem of defining boundary conditions at the exit plane. This work has addressed the issue and it is noted that a large length of computational domain can be used with fully developed flow boundary condition at the exit plane for low values of Reynolds number; for higher values of Re fully developed exit conditions are not exactly

satisfied when the electric field is present. However, if very small departures from zero radial velocity components at the exit plane are allowed, one can obtain approximate solutions, as has been done in some part of this work, which have excellent qualitative agreement with experiments on electro-convection.

References

Allen, P.H.G. and Karayiannis, T.G. (1995), "Electrohydrodynamic enhancement of Heat transfer and fluid flow", *Heat Recovery Systems and CHP*, Vol. 15 No. 5, pp. 389ff.

Chattock, A.P. (1899), "On the velocity and mass of ions in the electric wind air", *Phil. Magazine*, Vol. 48, pp. 401-20.

Fujino, T., Yokoyama, Y. and Mori, Y.H. (1989), "Augmentation of laminar forced-convective heat transfer by the application of a transverse electric field", *J. Heat Transfer*, Vol. 111, pp. 345-51.

Hauksbee, F. (1719), *Physico-Mechanical Experiments on Various Subjects*, London, pp. 46-7.

Kays, W.M. and Crawford, M.E. (1983), *Convective Heat and Mass Transfer*, T.M.H Publishing Co. Ltd, New Delhi.

Marco, S.M. and Velkoff, H.R. (1963), "Effect of electrostatic fields on free convection heat transfer from a flat plate", ASME Paper No. 63-HT-9.

Melcher, J.R. (1981), *Continuum Electromechanics*, MIT Press, Cambridge, MA.

Mizushina, T., Ueda, H., Matsumoto, T. and Waga, K. (1976), "Effect of electrically induced convection on heat transfer of air flow in an annulus", *J. Chem. Eng.*, Vol. 9, pp. 97-102.

Nag, A., Sarkar, A. and Sastri, V.M.K. (1993), "Natural convection in a differentially heated square cavity with a horizontal partition plate on the hot wall", *Comp. Methods Applied Mech. Eng.*, Vol. 110, pp. 143-56.

O'Brien and Shine (1967), "Effect of electrostatic fields on free convection heat transfer from a flat plate", *ASME J. Heat Transfer*, Vol. 89, pp. 114-5.

Ohadi, M.M., Nelson, D.A. and Zia, S. (1991), "Heat transfer enhancement of laminar and turbulent pipe flow via corona discharge", *Int. J. Heat Mass Transfer*, Vol. 34 Nos 4/5, pp. 1175-87.

Robinson, M. (1961), "Movement of air in the electric wind of the corona discharge", *Transactions of the American Institution of Engineers*, Vol. 80, pp. l43-150.

Seyed-Yagoobi, J. and Bryan, J.E. (1999), "Enhancement of heat transfer and mass transport in single-phase and two-phase flows with electrohydrodynamics", *Advances in Heat Transfer*, Academic press, New York, NY, Vol. 33.

Steutzer, O.M. (1959), "Ion drag pressure generation", *J. Appl. Phys.*, Vol. 30, pp. 984-94.

Yabe, A., Mori, Y. and Hijikata, K. (1978), "EHD study of the corona wind between wire and plate electrodes", *J. AIAA*, Vol. 16, pp. 340-5.

Zia, S. (1989), "Electrohydrodynamic heat transfer enhancement of forced convection in tubes, MS thesis Michigan Technological University, Houghton, Michigan.

Appendix. Electrodynamics

Coulomb's laws – related with force field with two point charges

$$F = \frac{Q_1 Q_2}{4\pi\varepsilon_0 r^2}$$

where ε_0 is the permittivity of free space; r the distance of separation; Q_1 and Q_2 are charges on two bodies whose sizes are small compared to the distance of separation; hence they are called "point charges".

The relevant units are F – newton (N); Q_1 and Q_2 – coulomb (C); r – meter (m) and ε_0 – $C^2/(N\,m^2)$.

In the case of the gravitational field of a material body, we define the "gravitational field intensity" as the force per unit mass experienced by a small test mass placed in that field. In a similar manner, the force per unit charge experienced by a small test charge placed in an electric field is known as the "electric field intensity", generally denoted by E.

So,

$$E = \frac{F}{Q_1} = \frac{Q_2}{4\pi\varepsilon_0 r^2};$$

in general,

$$E = \frac{Q}{4\pi\varepsilon_0 r^2}.$$

Unit of "E" is (N/C).

Now, if "ρ_e" represents charge per unit volume (i.e. charge density), the Coulomb force per unit volume$=E\rho_e=f_e$ (say)

Units: ρ_e – C/m^3 and f_e – N/m^3

This expression of "f_e" can be directly used in the usual expression of Navier-Stokes equation along with other body force terms. For this purpose, E and ρ_e need to be put down in the form of concerned variables (say, applied voltage).

Potential function (ϕ)

In fluid mechanics, we define $\vec{V} = \vec{\nabla}\phi$ where $\vec{V}$ stands for velocity vector and ϕ represents potential function (a scalar quantity).

Similarly, a body force potential can be defined such that when this potential is differentiated along a certain direction, the derivative will indicate the body force in that direction.

So, similarly, for this electric field, we can write, $\vec{E} = -\vec{\nabla}\phi$ where "ϕ" is called the electric potential. If we consider the variation of electric field intensity vector along the radial direction only,

then

$$E(r) = -\frac{\partial\phi}{\partial r} = -\frac{\mathrm{d}\phi}{\mathrm{d}r}$$

or

$$\int_\infty^r \mathrm{d}\phi = -\int_\infty^r E(r)\,\mathrm{d}r$$

or

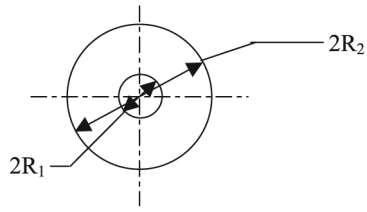

Figure A1.
The annulus

$$\phi(r) - \phi(\infty) = -\int_{\infty}^{r} \frac{Q}{4\pi\varepsilon_0 r^2}\,\mathrm{d}r \frac{Q}{4\pi\varepsilon_0 r}$$

If we define that $\phi(\infty) = 0$ (a chosen reference), then $\phi(r) = Q/4\pi\varepsilon_0 r$

In electrodynamics, a "displacement current density vector" ($\vec{D}$) is defined as $\vec{D} = \varepsilon_0 \vec{E}$

So, $\vec{D} = -\varepsilon_0 \vec{\nabla}\phi$

If "d" represents total displacement current across a section, then, $d = \vec{D} \cdot \vec{A}$

So,

$$|d| = -\varepsilon_0 \frac{\partial \phi}{\partial r} A_{\mathrm{r}} = -\varepsilon_0 2\pi r \frac{\partial \phi}{\partial r}$$

If $|d|$ is constant, then, we may write (Figure A1),

$$\mathrm{d}\phi = -\frac{|d|}{2\pi\varepsilon_0}\frac{\mathrm{d}r}{r} \quad \text{or} \quad \phi(R_2) - \phi(R_1) = \frac{|d|}{2\pi\varepsilon_0} \ln R_1/R_2$$

or

$$|d| = \frac{\phi(R_2) - \phi(R_1)}{\ln R_1/R_2}(2\pi\varepsilon_0)$$

So

$$|D(r)| = \frac{|d|}{A_{\mathrm{r}}} = \frac{\varepsilon_0}{r}\frac{\phi(R_2) - \phi(R_1)}{\ln R_1/R_2}$$

From the definition of $\vec{D}$ then

$$E(r) = \frac{1}{\varepsilon_0}|D_{\mathrm{r}}| = \frac{1}{\pi}\frac{\phi(R_2) - \phi(R_1)}{\ln R_1/R_2} \tag{A1}$$

This expression of $E(r)$ may be directly used in the computation of "f_{e}".

Now, we have to determine "ρ_{e}".

From Gauss' law,

$$\rho_{\mathrm{e}} = \bar{\nabla} \cdot \bar{D} = \bar{\nabla} \cdot (\varepsilon_0 \bar{E}) = \rho_0 \frac{\partial Er}{\partial r}$$

So,

$$\rho_{\mathrm{e}} = -\frac{\varepsilon_0}{r^2} A, \tag{A2}$$

where

$$A = \frac{\phi(R_2) - \phi(R_1)}{\ln R_1/R_2} \quad \text{(a constant for a given configuration).}$$

So, the electrical body force per unit volume (f_{e}) is expressed as

$$f_{\mathrm{e}} = \rho_{\mathrm{e}} E_{\mathrm{r}} = -\frac{\varepsilon_0 A^2}{r^3} \tag{A3}$$